Nanoscale

PAPER

Ullmann-type coupling of brominated tetrathienoanthracene on crystalline copper and silver†

Cite this: DOI: 10.1039/c3nr05710k

Rico Gutzler,*[ab] Luis Cardenas,*[ab] Josh Lipton-Duffin,[a] Mohamed El Garah,[a] Laurentiu E. Dinca,[a] Csaba E. Szakacs,[a] Chaoying Fu,[ab] Mark Gallagher,[c] Martin Vondráček,[d] Maksym Rybachuk,[ab] Dmitrii F. Perepichka*[b] and Federico Rosei*[a]

Received 25th October 2013
Accepted 5th December 2013

DOI: 10.1039/c3nr05710k

www.rsc.org/nanoscale

We report the synthesis of extended two-dimensional organic networks on Cu(111), Ag(111), Cu(110) and Ag(110) from thiophene-based molecules. A combination of scanning tunnelling microscopy and X-ray photoemission spectroscopy yields insight into the reaction pathways from single molecules towards the formation of two-dimensional organometallic and polymeric structures *via* Ullmann reaction dehalogenation and C–C coupling. The thermal stability of the molecular networks is probed by annealing at elevated temperatures of up to 500 °C. On Cu(111) only organometallic structures are formed, while on Ag(111) both organometallic and covalent polymeric networks were found to coexist. The ratio between organometallic and covalent bonds could be controlled by means of the annealing temperature. The thiophene moieties start degrading at 200 °C on the copper surface, whereas on silver the degradation process becomes significant only at 400 °C. Our work reveals how the interplay of a specific surface type and temperature steers the formation of organometallic and polymeric networks and describes how these factors influence the structural integrity of two-dimensional organic networks.

Introduction

Carbon–carbon coupling reactions on surfaces have been recently explored for the synthesis of one-dimensional (1D) and two-dimensional (2D) polymers.[1–8] Such atom-thick nanostructures derived from the covalent coupling of suitable precursor molecules are promising candidates for a variety of potential applications such as ultra-thin membranes for gas separation or as active elements in (opto)electronic devices.[9,10] Over the years a number of reaction mechanisms have been investigated for covalent coupling of molecular building blocks, with Ullmann-type reactions of halogenated aromatic molecules on metallic substrates being one of the most used method.[4,11–17] Other reactions for achieving surface-confined C–C coupling such as Sonogashira coupling of haloaromatics with a terminal alkyne,[18] alkane dehydrogenative polymerization[19,20] and oxidative terminal alkyne (Glaser–Hay) coupling[21–23] have been studied. In these examples, the surface acts as a constraint for the motion of the precursor molecules, confining the reaction to two dimensions. It can also act as a catalyst (*e.g.* in the cleavage of C–halogen bonds in the Ullmann reaction) and stabilizes intermediate reaction products.

The Ullmann reaction is the oldest known C–C coupling method for (halogenated) aromatic molecules.[24] It is understood to proceed *via* the oxidative addition of the catalyst (metallic copper) which inserts itself into the carbon–halogen bond, followed by reductive elimination ejecting the copper halide and forming a C–C bond.[25] It has been investigated by several surface-sensitive techniques[26,27] and has been demonstrated as a viable route for C–C coupling of polyhalogenated molecules on several transition metal surfaces: copper,[11,12,14,16,28] silver[12,13,29] and gold.[4,15,30–33] In the surface-confined version of the reaction, the first step of the reaction (dehalogenation of the molecule after which the halogen atoms adsorb onto the surface) is often observed to precede the C–C coupling.[11,13,14,27,33–35] It is generally assumed that the dehalogenated molecules form organometallic complexes with either metal adatoms[11,12,16,36] or directly with surface atoms.[28,29] However, the exact nature of the metal–carbon coordination complex is still controversial and may depend on the choice of substrate (*e.g.* compare findings reported in ref. 16 with ref. 37

[a]*Institut National de la Recherche Scientifique and Centre for Self-Assembled Chemical Structures, Université du Québec, 1650 Boulevard Lionel-Boulet, Varennes, QC J3X 1S2, Canada. E-mail: r.gutzler@fkf.mpg.de; cardenas@emt.inrs.ca; rosei@emt.inrs.ca*

[b]*Department of Chemistry and Centre for Self-Assembled Chemical Structures, McGill University, 801 Sherbrooke Str. West, Montreal, QC H3A 0B8, Canada. E-mail: dmitrii.perepichka@mcgill.ca*

[c]*Department of Physics, Lakehead University, 955 Oliver Road, Thunder Bay, ON P7B 5E1, Canada*

[d]*Fyzikální ústav AV ČR, v.v.i., Na Slovance 2, 182 21 Praha 8, Czech Republic*

† Electronic supplementary information (ESI) available: Additional STM data and DFT results. See DOI: 10.1039/c3nr05710k

for copper and ref. 12 and 38 with ref. 13 for silver). Annealing the surface can eventually lead to the breaking of the carbon–metal bonds and subsequent C–C coupling of molecules.[11–16,28–33] Since the Ullmann reaction typically requires high temperatures (~200 °C on copper),[24] the thermal stability of the precursor molecule and the resulting network becomes an important issue. Moreover, the role of the surface material itself in the reaction as a catalyst and as a stabilizing agent for intermediate reaction products has yet to be clarified, calling for an in-depth analysis.[12,23,28,39] Herein we address these two important topics by conducting a temperature-dependent study using Cu(111), Ag(111), Cu(110) and Ag(110) as supporting surfaces for the Ullmann coupling reaction.

Recently we have shown that surface-confined Ullmann polymerization can be extended to thiophene-containing monomers, which are among the most versatile building blocks for π-conjugated materials.[40] An epitaxial growth of ordered 1D poly(ethylenedioxy)thiophene (PEDOT) was observed on Cu(110).[14] However, using copper surfaces for polymerization of a brominated tetrathienoanthracene TBTTA (Scheme 1) failed to produce a 2D polymer. The increased annealing temperature required to rearrange the 2D organometallic intermediate into a conjugated polymer was hypothesized to cause desulfurization of the thiophene ring. Accordingly, the less reactive Ag(111) surface and higher temperature had to be used to accomplish covalent linking of TTA building blocks (Scheme 1).[17] To gain insight into the individual reaction steps of 2D polymerization, herein we report a temperature-dependent scanning tunnelling microscopy (STM) and X-ray photoemission spectroscopy (XPS) study of the reaction of TBTTA on Ag(111) and Cu(111) surfaces. Monitoring the evolution of the XPS spectra during annealing from 50 °C to 500 °C allows us to follow the reaction steps from the formation of organometallic intermediate structures to the formation of polymeric networks. Furthermore, we explore the competition between the desired formation of the 2D networks and the by-side desulfurization reaction that controls the overall stability of the thiophene-containing networks on metallic surfaces.

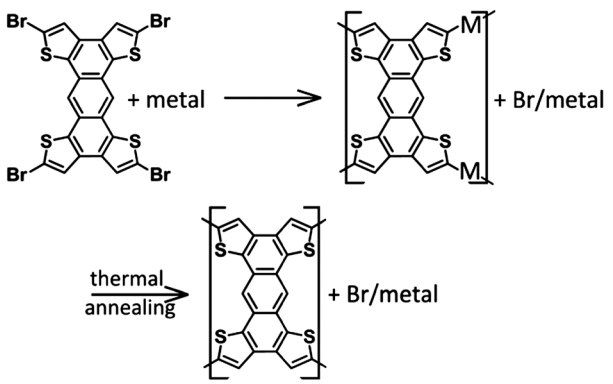

Scheme 1 TBTTA in the surface-confined Ullmann reaction from the precursor molecule to an organometallic intermediate, and to a π-conjugated covalent polymer.

Materials and methods

Prior to molecular deposition, Ag(111), Ag(110), Cu(111), and Cu(110) single crystals were cleaned by repeated cycles of sputtering with Ar^+ ions and subsequent annealing at 500 °C for Ag(111), Cu(111), and Cu(110) and 430 °C for Ag(110). TBTTA was sublimed from Knudsen cells at temperatures between 190 °C and 210 °C. The substrates were held at room temperature during deposition. Varying the sublimation temperature did not influence the structures observed after deposition. After sublimation of TBTTA, the samples were annealed for 10 minutes at various temperatures and investigated by STM and photoemission spectroscopy.

STM data were recorded at room temperature (unless otherwise specified) using commercial UHV systems (VT STM by Omicron GmbH and Arhus 150 STM by SPECS GmbH) using both etched tungsten and cut Pt/Ir tips. STM images were corrected to reflect the known substrate lattice parameters wherever possible to compensate for instrumental drift, using the free WSxM software[41] or the commercial SPIP software (Image Metrology A/S). Further image post-processing included plane subtraction and flattening.

High-resolution XPS measurements were performed at the Materials Science Beamline at the ELETTRA synchrotron, using a Phoibos 150 analyzer (SPECS GmbH). All spectra reported here were acquired in UHV with the sample held at room temperature after annealing at each temperature step for 10 minutes. Photon energies of 360 eV, 250 eV and 140 eV were used to record spectra from C 1s, S 2p, and Br 3d respectively. The spectra are all referenced to the Fermi level, measured after every spectrum, to determine absolute binding energies. Sample degradation due to X-ray irradiation was not observed. A smooth curve corresponding to the lineshape of the residual C 1s signal from each pristine substrate was subtracted to remove the background. Each of the C 1s spectra were decomposed into the same number of separate Voigt lineshapes. Once the optimum positions of the peaks were determined, their lineshape parameters (Gaussian and Lorentzian widths) were fixed across each substrate/monolayer dataset, and only intensities were allowed to vary to arrive at the best fit for each spectrum.

Results and discussion

Cu(111)

Deposition of TBTTA on Cu(111) leads to the formation of irregularly patterned networks (Fig. 1a) The composition of the network deposited at room temperature (Fig. 1a) changes only slightly after annealing at 150 °C for 10 minutes (Fig. 1b). However, the borders of the network become poorly defined after annealing at 250 °C (Fig. 1c), which can be related to the rupture of the molecules in the network (*vide infra*). No evidence of a covalent TTA polymer (final product of the C–C coupling) was observed by STM. The networks exhibit occasional local arrangement of molecules in ordered structures over an extent of several nanometers (Fig. 2a and b). One of these ordered networks is a Kagome lattice with a hexagonal unit cell, the other is a twofold symmetric structure with an oblique unit cell

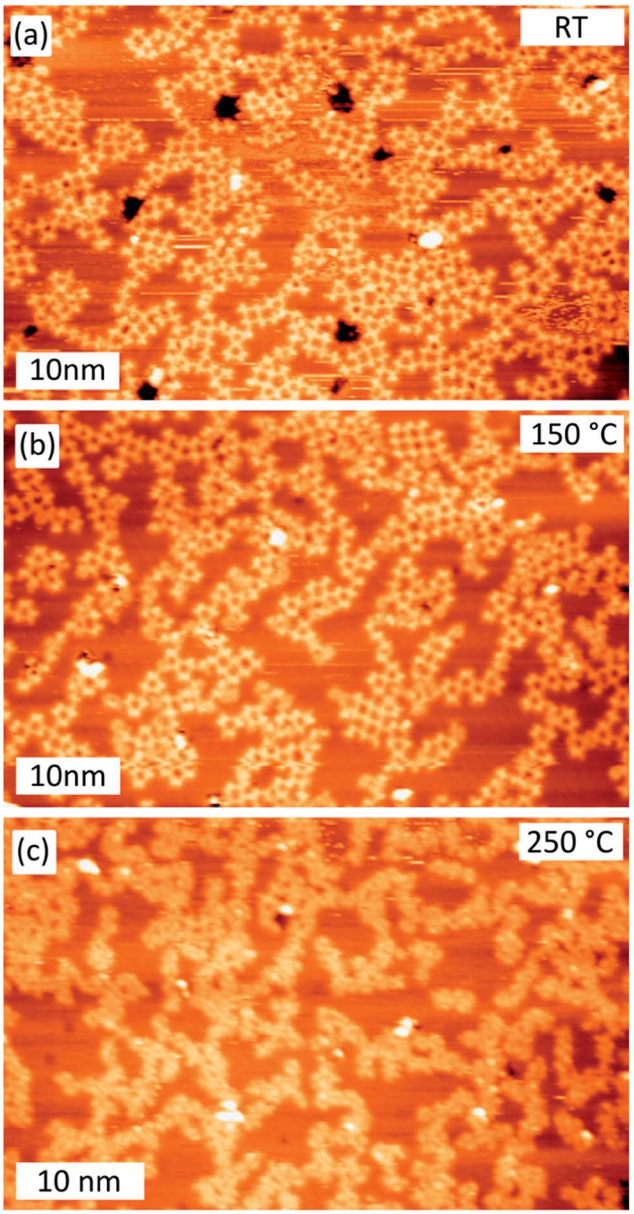

Fig. 1 Overview images of TBTTA on Cu(111) as deposited at (a) room temperature ($U_{bias} = -2000$ mV, $I_{tunnel} = 0.590$ nA), (b) after annealing at 150 °C ($U_{bias} = -1600$ mV, $I_{tunnel} = 0.430$ nA), and (c) after annealing at 250 °C ($U_{bias} = -1900$ mV, $I_{tunnel} = 0.370$ nA) for 10 minutes.

(Fig. 2a). The oblique structure is already present at RT (Fig. 1a), while the Kagome lattice appears subsequent to annealing at 200 °C for 10 minutes. The dimensions of the Kagome lattice, which can be accurately deduced from images in which both the molecular suprastructure and the atomically resolved Cu(111) substrate are simultaneously observed (Fig. 2b), suggest that it is an organometallic network with TTA fragments bridged by copper atoms. The unit cell is 2.7 ± 0.1 nm in size, in perfect agreement with the 2.70 nm predicted by density functional theory (DFT) calculations of this structure (see ESI;† a distance of 2.21 nm is expected for a Kagome network comprising TTA–TTA covalent links). Similar geometric considerations lead to

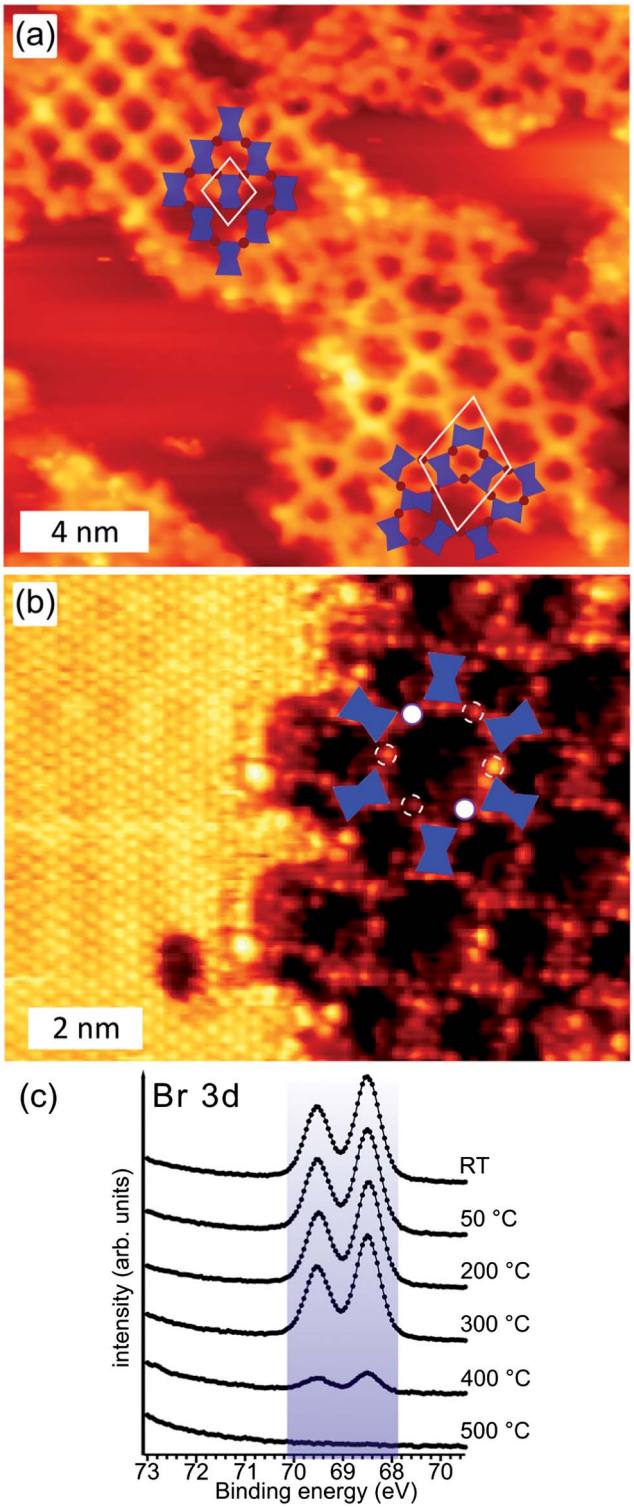

Fig. 2 (a) STM micrograph of the oblique structure (upper left) and Kagome lattice (lower right) with molecular models of the organometallic networks (unit cells are depicted in white, blue polygons represent TTA molecules). Surrounding these ordered patches are molecules adsorbed in a disordered fashion ($U_{bias} = -2000$ mV, $I_{tunnel} = 0.960$ nA). (b) STM micrograph of the Kagome lattice with an atomically resolved Cu(111) lattice ($U_{bias} = -396$ mV, $I_{tunnel} = 1.028$ nA). Coordinated Cu adatoms between molecules are discernible as circular protrusions. (c) XPS spectra of the Br 3d core level on Cu(111) for room temperature and all annealing temperatures.

the conclusion that the oblique structure is also organometallic and is stabilized by coordinated metal centers; its unit cell measures $a = b = 1.4 \pm 0.1$ nm, in agreement with DFT calculations (ESI†).

Core level spectroscopy was used to follow the progress of the reaction at various temperatures in the 50 °C to 500 °C range. The Br 3d core level plotted in Fig. 2d for various temperatures indicates that debromination of TBTTA is already complete at room temperature on Cu(111): the 3d core level consists of a single doublet with the $3d_{5/2}$ peak at 68.5 eV, which is below the expected value of carbon-bonded bromine (69.6 eV (ref. 15 and 42–44)) but is consistent with chemisorbed bromine.[35] The position of the Br 3d doublet does not change upon annealing, although the peak intensity decreases, indicating an onset of Br desorption at ~400 °C.

The C 1s core level spectrum of the TBTTA sample deposited at room temperature is centered at 284.7 eV with a shoulder at low binding energy (Fig. 3). Debromination is supported by the absence of a contribution from C–Br bonds, which is expected at high binding energy above 286 eV.[35,43,44] The shoulder at lower binding energy (green curve) can be attributed to C–Cu bonds[45–47] in the organometallic structures which are observed by STM. The electropositive metal leads to additional charge in the molecule, which lowers the binding energy of the core levels. The central part of the XPS signal (red curve), with its maximum at 284.7 eV is consistent with sp^2 C contributions as observed for other thiophene derivatives.[48–51] We furthermore note the appearance of a high-energy contribution (blue curve) starting at 200 °C, which we tentatively attribute to the formation of C–S–metal bonds formed once the thiophene units disintegrate (see below).

Annealing at 200 °C shifts the entire spectrum to lower binding energies, suggesting an increase of the negative charge on TTA carbons. This can be interpreted as a result of additional bonding of TTA to electropositive copper atoms.[39]

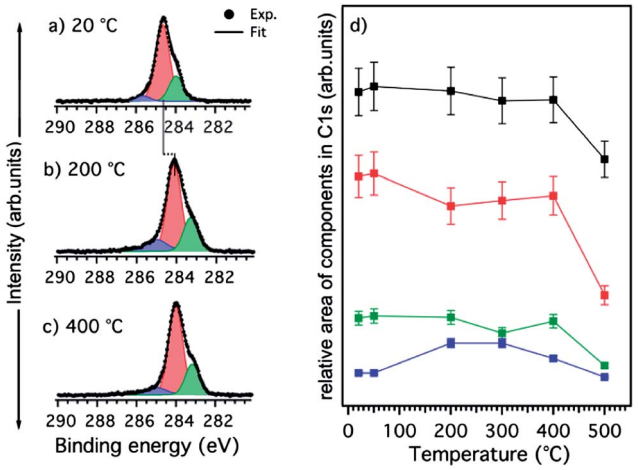

Fig. 3 C 1s core level on Cu(111) for (a) room temperature as deposited, (b) after annealing at 200 °C and (c) after annealing at 400 °C for 10 minutes. The evolution of each contribution with annealing temperature is plotted in (d). (Total signal: black curve, Voigt fits in blue, red, and green.)

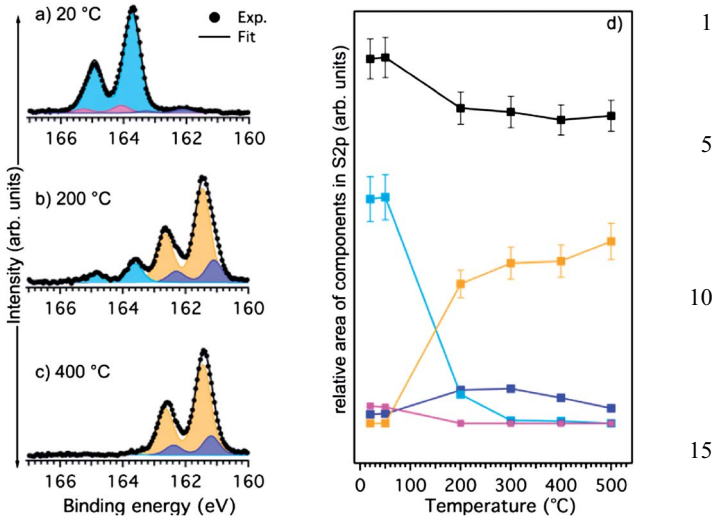

Fig. 4 S 2p core level spectra for TBTTA on Cu(111). (a) After deposition of TBTTA without annealing. (b) After annealing at 200 °C and (c) after annealing at 400 °C for 10 minutes. (d) Areas of different contributions after deconvolution for all annealing temperatures.

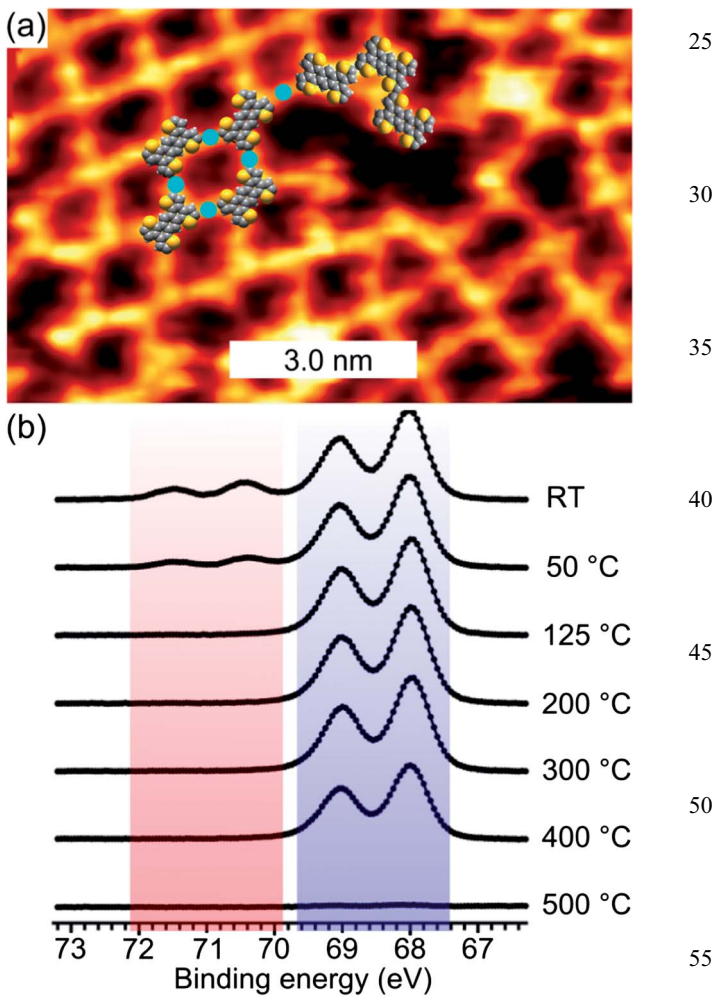

Fig. 5 (a) STM image of the 2D network on Ag(111) ($U_{bias} = -758$ mV, $I_{tunnel} = 0.877$ nA). (b) Core level spectra of the Br 3d level on Ag(111) at room temperature and various annealing temperatures up to 500 °C.

The origin of this shift can be understood by analyzing the S 2p core level spectra: as discussed below, the C–S bond of the thiophene ring starts to break above 200 °C, which leads to rebonding of the carbon and sulfur atoms to the electropositive copper atoms.

The shift in the C 1s signal occurs at the same annealing temperature (~200 °C) at which the S 2p spectrum (Fig. 4) begins to change considerably. At room temperature (Fig. 4a), we observe a dominant doublet state at 163.7 eV ($2p_{3/2}$ position, light blue curve) which corresponds to sulfur in the intact (but dehalogenated) TTA molecules.[49–52] At 200 °C (Fig. 4b), one intense additional doublet is found at much lower binding energy around 161.4 eV (yellow). This lower-energy peak originates from sulfur in broken thiophene units as C–S–Cu (thiolate) (the smaller doublet at 161.1 eV (violet curve) likely originates from atomically adsorbed sulfur).[50,52,53] By comparing the evolution of C 1s and S 2p spectra, we observe the complete rupture of the thiophene units between 200 and 300 °C. A similar rupture of the thiophene unit in TTA has also been observed on Ni(111) in which case it leads to a cyclization reaction converting the desulfurized TTA into pentacene.[54]

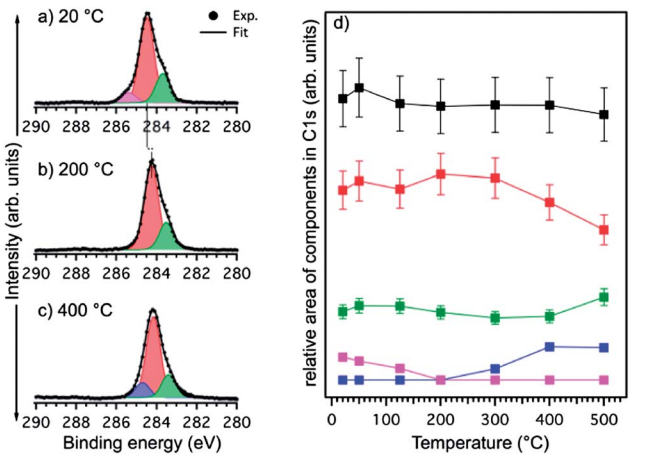

Fig. 6 C 1s core level on Ag (111) at (a) room temperature and after annealing at (b) 200 °C and (c) 400 °C. (d) Peak-area evolution as a function of annealing temperature.

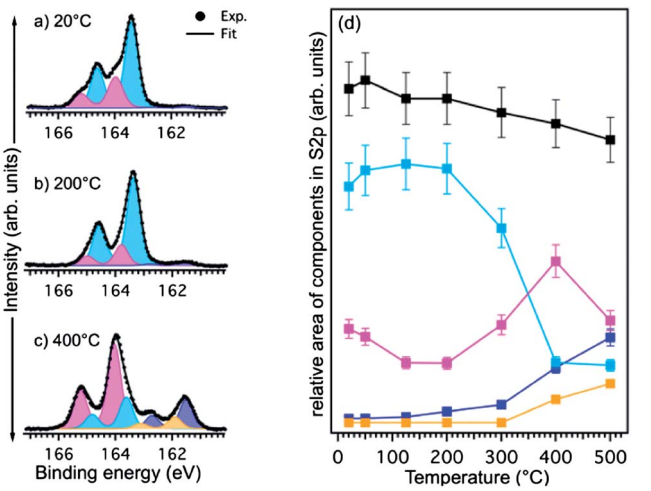

Fig. 7 S 2p core level for Ag(111). (a) Sample after deposition of TBTTA without annealing. (b) After annealing at 300 °C and (c) after annealing at 400 °C. (d) Area of different contributions after deconvolution for all annealing temperatures.

Ag(111)

In contrast to the case of Cu(111), the adsorption of TBTTA on Ag(111) and subsequent annealing at 300 °C for 10 minutes leads to the formation of both polymeric and organometallic networks co-observed in the same STM images (Fig. 5a). The synthesis and characterization of these porous polymeric networks is discussed in detail elsewhere.[17]

A series of Br 3d core level spectra acquired as a function of annealing temperature on Ag(111) is displayed in Fig. 5b. In contrast to the Cu(111) experiments above, a high binding energy doublet due to the presence of bromine in C–Br bonds ($3d_{5/2}$ peak at 70.4 eV, red, 17% of total signal area),[15,42–44] is observed immediately after deposition at RT. It remains observable after annealing up to 50 °C but disappears completely at 125 °C. Above this temperature, the only contribution stems from chemisorbed Br on the silver surface, with $3d_{5/2}$ at 68.0 eV (blue).[55] The intensity of the Br–Ag contribution diminishes with further increase of annealing temperature; as in the case of Cu(111), at 500 °C no Br is left on the Ag surface.

Fig. 6 shows a series of C 1s core level spectra of TBTTA on Ag(111) as a function of annealing temperature. Similar contributions to those encountered on Cu(111) can be identified to arise from the different carbon atoms present in the molecule.[48–51] A small signal at high binding energy (magenta curve, 285.3 eV) observed at lower temperatures is likely due to C–Br bonds. This signal is drastically reduced above 125 °C, in agreement with the interpretations made from the Br 3d spectra.‡

More insight into the stability of the polymeric networks can be obtained from the S 2p spectra (Fig. 7). Two doublets observed at room temperature ($2p_{3/2}$ at 163.9 eV and 163.4 eV) correspond to sulfur atoms in partially dehalogenetad TTA (see below).[49–52] Two additional doublets at lower binding energies of 162.0 eV and 161.5 eV appear after annealing at 300 °C. These peaks are attributed to sulfur in a partially broken thiophene ring as C–S–Ag bonds and to chemisorbed sulfur on the Ag(111) surface and indicate rupture of the molecule at its thiophene units.[50,52,53] Even annealing up to 500 °C leads to the rupture of only a limited fraction of thiophene groups (~1/3, *cf.* Fig. 7d). This is a significant difference with respect to copper for which no intact thiophene groups were observed above 200 °C.

‡ A quantitative discussion of peak intensities or areas is hindered by possible photoelectron diffraction, which can significantly alter the intensity ratios. Backscattering can occur in ordered structures of Br–Ag which is not expected in Br–C in the intact TBTTA molecule [A.-B. Yang, F. C. Brown, J. J. Rehr, M. G. Mason and Y. T. Tan, *Phys. Rev. B: Condens. Matter Mater. Phys.*, 1992, **44**, 6188]. This would explain the lower ratio of Br–C to Br–Ag contribution in Br 3d (~1/5) compared to Br–C to C–Ag in C 1s (~1/3).

The two separate high-energy contributions at 163.9 eV and 163.4 eV are attributed to two distinct chemical environments of the thiophene unit in polymeric and organometallic networks, respectively (halogenated TBTTA is also expected at 163.9 eV). In the organometallic structure, the S 2p core levels are screened due to electropositive metal atoms, resulting in a shift to lower binding energy with respect to the TBTTA monomer or polymeric network.§ Based on the premise of two different S 2p signals for organometallic and polymeric structures (Fig. 7), we can estimate their relative appearance on the surface by calculating the ratio between the areas underneath both peaks. Up to 200 °C, the ratio is about 1 : 4 polymer : organometallic. Above 300 °C the ratio is approaching 1 : 1, which correlates well with the ratio extracted from the analysis of STM images.[17] Annealing at 400 °C not only leads to a higher degree of polymerization with respect to the organometallic precursor state, but also brings about a considerable amount of desulfurization (Fig. 7d), which limits the complete transformation of the organometallic structure into polymer.

Cu (110) and Ag(110)

In addition to the elementary composition of the surface as described above, surface-confined reactions can also be influenced by the crystal facet. This point was addressed by the deposition of TBTTA onto the low-index surfaces Cu(110) and Ag(110) at room temperature. On Cu(110) the debrominated molecules orient with their long axis parallel to the [001] lattice vector of the copper substrate (Fig. 8a). Two molecules likely coordinate a copper atom and are separated by 1.5 nm, which agrees with the distance calculated for organometallic compounds (1.45 nm, see the discussion of Cu(111)). Surrounding the dimer, four protrusions are observed (white arrows), all of which occupy the same adsorption site of the Cu(110) lattice, and which we speculate are coadsorbed bromine atoms. In certain regions of the substrate the binding motif results in domains of ordered organometallic structures (Fig. 8b), in which one-dimensional organometallic rows align in parallel. In analogy with Cu(111), annealing the Cu(110) surface did not lead to covalent C–C coupling. Preferential 1D diffusion of TTA on the (110) facet is likely responsible for different networks that form on Cu(110) *vs.* Cu(111).

On Ag(110), deposition of TBTTA at RT leads to the formation of islands of a porous organometallic network (Fig. 9a). After annealing at 300 °C, disordered covalent networks are formed (Fig. 9e and g). The distance between molecules in these structures (1.2 ± 0.1 nm, Fig. 9g and ESI†) is in agreement with the polymers observed on Ag(111) and with gas-phase DFT calculations. At intermediate annealing temperatures of 200 °C

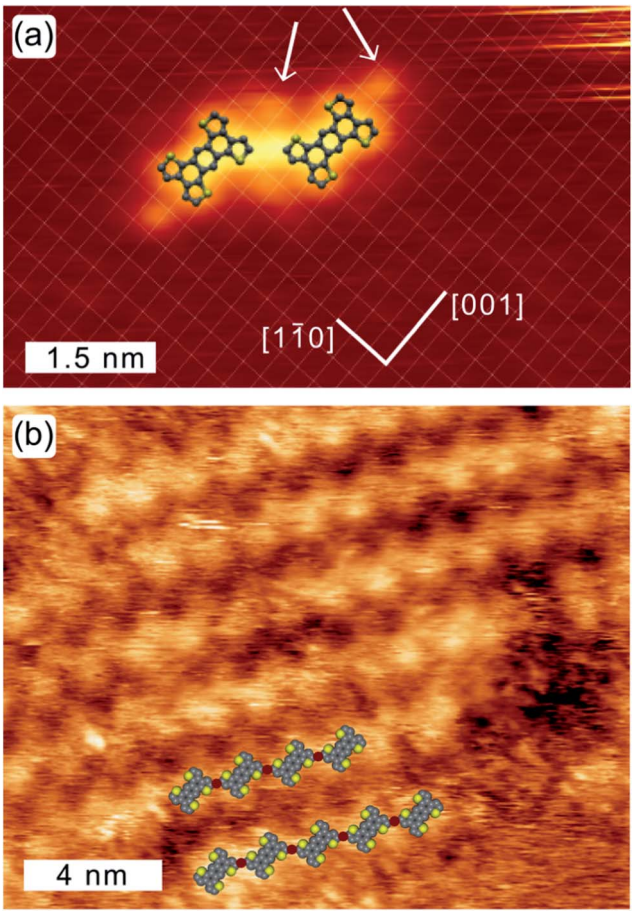

Fig. 8 (a) STM micrograph of two TTA molecules on Cu(110) (U_{bias} = −1500 mV, I_{tunnel} = 0.086 nA). The dimer coordinates one copper atom. Four Br atoms are adsorbed close to the dimer (two of which indicated by white arrows). The underlying Cu(110) lattice (see ESI† for the STM image with atomic resolution) allows for calibration of the intermolecular distance (1.5 nm). (b) 1D organometallic chains on Cu(110) (U_{bias} = −700 mV, I_{tunnel} = 0.562 nA).

two types of well-ordered islands are observed, which were absent at both room temperature and after annealing at higher temperatures (structures I and II, Fig. 9b–d). The two ordered structures display different unit cells, and individual TTA molecules are readily identifiable. The unit cell of structure I measures 1.0 × 1.3 nm^2 with an angle of 123°, whereas the unit cell of structure II measures 1.7 × 1.1 nm^2, 105°. Each unit cell additionally comprises small circular protrusions surrounding the molecules, which we tentatively attribute to chemisorbed bromine atoms that are detached from the molecule. These protrusions are reminiscent of features observed in the dehalogenation and polymerization of aryl-halides in 1D.[11,35,38] The dehalogenated molecules are stabilized by covalent bonds with silver surface atoms. This type of intermediate step in the reaction from the brominated molecule to polymer has been observed previously in the synthesis of porous graphene from iodo-substituted cyclohexa-*m*-phenylene on Ag(111).[13,28] In these studies Bieri *et al.* show that prior to aryl–aryl coupling, dehalogenated macrocycles adsorb onto the surface forming bonds with metal atoms. They also observe decoupled iodine in close

§ The shift in a core level due to the 2nd nearest-atoms, in this case in a C–C–S *vs.* a Ag–C–S bonding environment, is a frequently studied effect. [R. L. Opila, G. D. Wilk, M. A. Alam, R. B. van Dover, B. W. Busch *et al.*, *Appl. Phys. Lett.*, 2002, **81**, 1788]. In addition, we addressed the feasibility of chemical shifts induced in the S 2p core level through changes in the chemical environment of neighboring C atoms by DFT (see ESI†). This analysis indicates that shifts up to 1 eV are possible by changing from organometallic to covalent polymeric bonds.

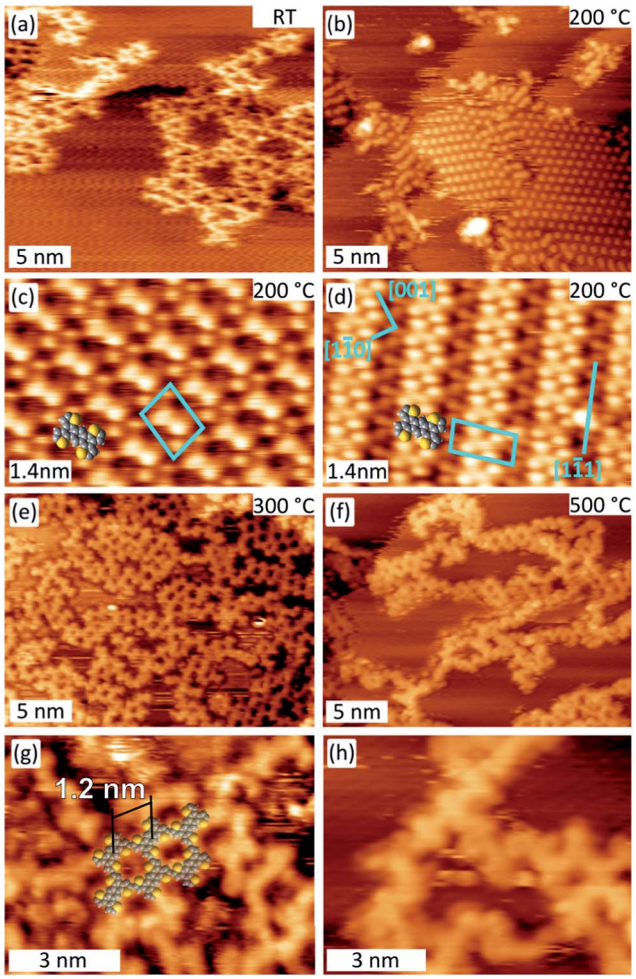

Fig. 9 TBTTA deposited onto Ag(110) held at room temperature. (a) Without annealing, recorded at −175 °C (U_{bias} = 508 mV, I_{tunnel} = 0.780 nA). (b) Ordered organometallic structures after annealing at 200 °C recorded at room temperature (U_{bias} = −432 mV, I_{tunnel} = 0.260 nA), (c) close up on structure I (U_{bias} = −1201 mV, I_{tunnel} = 0.180 nA) and (d) structure II (U_{bias} = −1583 mV, I_{tunnel} = 1.260 nA), with the unit cell given in blue. (e and g) Disordered polymer after annealing at 300 °C (U_{bias} = 884 mV, I_{tunnel} = 0.330 nA), and (f and h) degraded structure after annealing at 500 °C (U_{bias} = −558 mV, I_{tunnel} = 0.460 nA).

proximity to the dehalogenated molecule. Similar close adsorption of halogen atoms after dissociation from the molecule was reported by Lipton-Duffin *et al.* for diiodobenzene on Cu(110).[11] A detailed analysis of this structure is given in the ESI,† which features DFT calculations including the surface. None of the ordered structures persists at elevated annealing temperatures; at 300 °C, molecules bind covalently to their neighbors and form extended polymeric networks. As on Ag(111), almost full coverage of the crystal surface by the organic network is achieved (see ESI†). The disordered nature of the covalent network is due to a large number of possible crystallographic defects that can be formed by connecting TTA in several different arrangements. A detailed discussion of defects in TTA polymers can be found in ref. 17. Annealing the substrate to even higher temperatures of up to 500 °C leads to decomposition of the molecular network (Fig. 9f and h).

Conclusions

Combined STM and XPS monitoring of the Ullmann reaction of TBTTA on Cu(111) and Ag(111) reveals how the supporting substrate and the temperature influence the reaction steps and the formation of by-products. XPS confirms the dehalogenation of TBTTA, which occurs completely at room temperature on Cu(111) yet requires additional thermal energy on Ag(111), in line with the higher reactivity of the former. Chemisorbed Br remains on the surface up to high temperatures and an onset of desorption is observed at 400 °C. STM results reveal that dehalogenation of TBTTA on copper leads to the formation of organometallic networks in which copper adatoms are coordinated in a network of debrominated molecules. It was found that C–C coupling polymerization cannot be selectively induced by thermal annealing due to the breaking of the thiophene units at ≥200 °C. On Ag(111), annealing at 300 °C induces the formation of a mixture of disordered planar organometallic and covalent polymeric networks without rupturing the thiophene units. Annealing at even higher temperatures further increases the fraction of the polymeric network, although partial cleavage of the thiophene unit also becomes apparent. The same transition at elevated temperatures from organometallic intermediates to polymeric networks is observed for the Ag(110) surface, while in analogy to Cu(111) only organometallic chains with coadsorbed Br atoms are observed on Cu(110).

The synthesis of surface-supported 2D polymers is shown to depend strongly on the type of substrate chosen. This is especially important for surface-confined polymerization of structurally complex π-functional monomers. For thiophene-containing structures (the most widespread building block used in the synthesis of π-conjugated polymers) the choice of catalytic surface affects the integrity of the polymer: on copper the thiophene unit is not stable at temperatures required for the transformation of organometallic intermediates into 2D covalent polymers. However, the polymerization through C–C coupling can be induced on silver without degradation of the molecular building units. Thus, a trade-off must be found between the catalytic activity of the substrate and the stability of the molecule/polymer. The optimal conditions will likely be monomer-specific and thus temperature dependent studies are important for understanding the formation of different functional polymers.

Acknowledgements

Rico Gutzler and Luis Cardenas contributed equally to this work. This work was supported by the Natural Sciences and Engineering Research Council of Canada (NSERC) through Discovery Grants, as well as the Fonds Quebecois sur la Recherche en Nature et Technologies (FQRNT) through a Team Grant and the Ministère du Développement Economique, de l'Innovation et de l'Exportation (MDEIE) through an international collaboration Grant. We thank the Centre for Research in Molecular Modelling (CERMM) for access to computational infrastructure. The Materials Science Beamline and MV are supported by the Ministry of Education of the Czech Republic

under grants LG12003 and LM2011029. LC is grateful to FRSQ for a post-doctoral fellowship. MG thanks the ACS Petroleum Research Fund for a summer fellowship. FR is grateful to the Canada Research Chairs program for partial salary support and to the Alexander von Humboldt Foundation for a FW Bessel Award. LED acknowledges a graduate fellowship from FRQNT. This work was partly supported by Elsevier through a grant from Applied Surface Science.

Notes and references

1 C.-A. Palma and P. Samorì, *Nat. Chem.*, 2011, **3**, 431–436.
2 M. Lackinger and W. M. Heckl, *J. Phys. D: Appl. Phys.*, 2011, **44**, 464011.
3 G. Franc and A. Gourdon, *Phys. Chem. Chem. Phys.*, 2011, **13**, 14283–14292.
4 L. Grill, M. Dyer, L. Lafferentz, M. Persson, M. V. Peters and S. Hecht, *Nat. Nanotechnol.*, 2007, **2**, 687–691.
5 N. R. Champness, *Nat. Nanotechnol.*, 2007, **2**, 671–672.
6 L. Bartels, *Nat. Chem.*, 2010, **2**, 87–95.
7 A. Gourdon, *Angew. Chem., Int. Ed.*, 2008, **47**, 6950–6953.
8 M. El Garah, J. M. MacLeod and F. Rosei, *Surf. Sci.*, 2013, **613**, 6–14.
9 D. F. Perepichka and F. Rosei, *Science*, 2009, **323**, 216–217.
10 J. W. Colson and W. R. Dichtel, *Nat. Chem.*, 2013, **5**, 453–465.
11 J. A. Lipton-Duffin, O. Ivasenko, D. F. Perepichka and F. Rosei, *Small*, 2009, **5**, 592–597.
12 R. Gutzler, H. Walch, G. Eder, S. Kloft, W. M. Heckl and M. Lackinger, *Chem. Commun.*, 2009, 4456–4458.
13 M. Bieri, M. Treier, J. Cai, K. Aït-Mansour, P. Ruffieux, O. Gröning, P. Gröning, M. Kastler, R. Rieger, X. Feng, K. Müllen and R. Fasel, *Chem. Commun.*, 2009, 6919–6921.
14 J. A. Lipton-Duffin, J. A. Miwa, M. Kondratenko, F. Cicoira, B. G. Sumpter, V. Meunier, D. F. Perepichka and F. Rosei, *Proc. Natl. Acad. Sci. U. S. A.*, 2010, **107**, 11200–11204.
15 S. A. Krasnikov, C. M. Doyle, N. N. Sergeeva, A. B. Preobrajenski, N. A. Vinogradov, Y. N. Sergeeva, A. A. Zakharov, M. O. Senge and A. A. Cafolla, *Nano Res.*, 2011, **4**, 376–384.
16 W. Wang, X. Shi, S. Wang, M. A. Van Hove and N. Lin, *J. Am. Chem. Soc.*, 2011, **133**, 13264–13267.
17 L. Cardenas, R. Gutzler, J. Lipton-Duffin, C. Fu, J. L. Brusso, L. E. Dinca, M. Vondráček, Y. Fagot-Revurat, D. Malterre, F. Rosei and D. F. Perepichka, *Chem. Sci.*, 2013, **4**, 3263–3268.
18 V. K. Kanuru, G. Kyriakou, S. K. Beaumont, A. C. Papageorgiou, D. J. Watson and R. M. Lambert, *J. Am. Chem. Soc.*, 2010, **132**, 8081–8086.
19 D. Zhong, J.-H. Franke, S. K. Podiyanachari, T. Blömker, H. Zhang, G. Kehr, G. Erker, H. Fuchs and L. Chi, *Science*, 2011, **334**, 213–216.
20 M. In't Veld, P. Iavicoli, S. Haq, D. B. Amabilino and R. Raval, *Chem. Commun.*, 2008, 1536–1538.
21 Y.-Q. Zhang, N. Kepčija, M. Kleinschrodt, K. Diller, S. Fischer, A. C. Papageorgiou, F. Allegretti, J. Björk, S. Klyatskaya, F. Klappenberger, M. Ruben and J. V. Barth, *Nat. Commun.*, 2012, **3**, 1286.
22 J. Eichhorn, W. M. Heckl and M. Lackinger, *Chem. Commun.*, 2013, **49**, 2900–2902.
23 H.-Y. Gao, H. Wagner, D. Zhong, J.-H. Franke, A. Studer and H. Fuchs, *Angew. Chem., Int. Ed.*, 2013, **52**, 4024–4028.
24 F. Ullmann and J. Bielecki, *Ber. Dtsch. Chem. Ges.*, 1901, **34**, 2174–2185.
25 J. Hassan, M. Sévignon, C. Gozzi, E. Schulz and M. Lemaire, *Chem. Rev.*, 2002, **102**, 1359–1469.
26 S.-W. Hla, L. Bartels, G. Meyer and K.-H. Rieder, *Phys. Rev. Lett.*, 2000, **85**, 2777–2780.
27 M. M. Blake, S. U. Nanayakkara, S. A. Claridge, L. C. Fernández-Torres, E. C. H. Sykes and P. S. Weiss, *J. Phys. Chem. A*, 2009, **113**, 13167–13172.
28 M. Bieri, M.-T. Nguyen, O. Gröning, J. Cai, M. Treier, K. Aït-Mansour, P. Ruffieux, C. A. Pignedoli, D. Passerone, M. Kastler, K. Müllen and R. Fasel, *J. Am. Chem. Soc.*, 2010, **132**, 16669–16676.
29 M. Bieri, S. Blankenburg, M. Kivala, C. A. Pignedoli, P. Ruffieux, K. Müllen and R. Fasel, *Chem. Commun.*, 2011, **47**, 10239–10241.
30 M. O. Blunt, J. C. Russell, N. R. Champness and P. H. Beton, *Chem. Commun.*, 2010, **46**, 7157–7159.
31 L. Lafferentz, V. Eberhardt, C. Dri, C. Africh, G. Comelli, F. Esch, S. Hecht and L. Grill, *Nat. Chem.*, 2012, **4**, 215–220.
32 A. Saywell, J. Schwarz, S. Hecht and L. Grill, *Angew. Chem., Int. Ed.*, 2012, **51**, 5096–5100.
33 S. Schlögel, W. M. Heckl and M. Lackinger, *Surf. Sci.*, 2012, **606**, 999–1004.
34 G. S. McCarty and P. S. Weiss, *J. Am. Chem. Soc.*, 2004, **126**, 16772–16776.
35 M. Di Giovannantonio, M. El-Garah, J. Lipton-Duffin, V. Meunier, L. Cardenas, Y. Fagot Revurat, A. Cossaro, A. Verdini, D. F. Perepichka, F. Rosei and G. Contini, *ACS Nano*, 2013, **7**, 8190–8198.
36 H. Walch, R. Gutzler, T. Sirtl, G. Eder and M. Lackinger, *J. Phys. Chem. C*, 2010, **114**, 12604–12609.
37 M.-T. Nguyen, C. A. Pignedoli and D. Passerone, *Phys. Chem. Chem. Phys.*, 2011, **13**, 154–160.
38 K.-H. Chung, B.-G. Koo, H. Kim, J. K. Yoon, J.-H. Kim, Y.-K. Kwon and S.-J. Kahng, *Phys. Chem. Chem. Phys.*, 2012, **14**, 7304–7308.
39 J. Björk, F. Hanke and S. Stafström, *J. Am. Chem. Soc.*, 2013, **135**, 5768–5775.
40 *Handbook of Thiophene-Based Materials: Applications in Organic Electronics and Photonics*, ed. I. F. Perepichka and D. F. Perepichka, John Wiley & Sons, 2009.
41 I. Horcas, R. Fernández, J. M. Gómez-Rodríguez, J. Colchero, J. Gómez-Herrero and A. M. Baro, *Rev. Sci. Instrum.*, 2007, **78**, 013705.
42 A. C. Brieva, C. Jäger, F. Huisken, L. Šiller and Y. V. Butenko, *Carbon*, 2009, **47**, 2812–2820.
43 J.-F. Colomer, R. Marega, H. Traboulsi, M. Meneghetti, G. Van Tendeloo and D. Bonifazi, *Chem. Mater.*, 2009, **21**, 4747–4749.
44 S. Hanelt, J. F. Friedrich, G. Orts-Gil and A. Meyer-Plath, *Carbon*, 2012, **50**, 1373–1385.

45 J. M. Lindquist and J. C. Hemminger, *Chem. Mater.*, 1989, **1**, 72–78.
46 X.-L. Zhou and J. M. White, *J. Chem. Phys.*, 1990, **92**, 5612–5621.
47 X.-L. Zhou and J. M. White, *Catal. Lett.*, 1989, **2**, 375–384.
48 X. Liu, M. Knupfer and B.-H. Huisman, *Surf. Sci.*, 2005, **595**, 165–171.
49 F. Elfeninat, C. Fredriksson, E. Sacher and A. Selmani, *J. Chem. Phys.*, 1995, **102**, 6153–6158.
50 F. Terzi, L. Pasquali, M. Montecchi, S. Nannarone, A. Viinikanoja, T. Ääritalo, M. Salomäki, J. Lukkari, B. P. Doyle and R. Seeber, *J. Phys. Chem. C*, 2011, **115**, 17836–17844.
51 T. Schwieger, X. Liu, H. Peisert, B. Adolphi, N. Kiriy and M. Knupfer, *J. Appl. Phys.*, 2005, **97**, 123712.
52 G. Liu, J. A. Rodriguez, J. Dvorak, J. Hrbek and T. Jirsak, *Surf. Sci.*, 2002, **505**, 295–307.
53 D. L. Pugmire, M. J. Tarlov, R. D. van Zee and J. Naciri, *Langmuir*, 2003, **19**, 3720–3726.
54 L. E. Dinca, C. Fu, J. M. MacLeod, J. Lipton-Duffin, J. L. Brusso, C. E. Szakacs, D. Ma, D. F. Perepichka and F. Rosei, *ACS Nano*, 2013, **7**, 1652–1657.
55 M. K. Wagner, J. C. Hansen, R. DeSouza-Machado, S. Liang, J. G. Tobin, M. G. Mason, S. Brandt, Y. T. Tan, A.-B. Yang and F. C. Brown, *Phys. Rev. B: Condens. Matter Mater. Phys.*, 1991, **43**, 6405–6410.